Materials Advances

ROYAL SOCIETY OF CHEMISTRY

PAPER

View Article Online
View Journal | View Issue

Check for updates

Cite this: *Mater. Adv.*, 2026, 7, 1814

Covalent surface functionalization of carbon nitrides: a case study of poly(heptazine imide)

Florian Binder, [ab] Igor Moudrakovski, [a] Nils L. Kötter, [b] Saunak Das, [a] Kathrin Küster, [a] Sebastian Bette [a] and Bettina V. Lotsch *[ab]

Surface functionalization of graphitic carbon nitrides has been demonstrated to promote catalytic properties but has rarely been investigated with the 2D carbon nitrides poly(heptazine imide) (PHI) and poly(triazine imide) (PTI) despite their potential for a variety of applications. This may originate from the chemically inert and hence unreactive character of carbon nitrides in conjunction with the lack of possibilities to verify the success of a post-synthetic covalent functionalization. Herein, we address these problems and mainly investigate the possibility of covalently functionalizing PHI with any desired organic molecule. A strategy of using fluorine-containing functionalizations to enable access to ^{19}F NMR studies is utilized, which ensures the complete removal of unreacted functional groups (FGs) and provides an easy and reliable quantification of the functionalization afterwards. Screening experiments illustrate the necessity to increase the accessibility to the surface. Furthermore, a high yield can be achieved by using acyl chlorides as functionalization agents. In addition, the proof of covalent functionalization is provided by means of 2D NMR on ^{15}N-enriched PHI modified with a ^{13}C-enriched FG. Our study thus presents a general route to the covalent functionalization of PHI and opens up new perspectives for rationally adding desired functionality to polymeric carbon nitrides in general.

Received 19th November 2025,
Accepted 25th December 2025

DOI: 10.1039/d5ma01345c

rsc.li/materials-advances

Open Access Article. Published on 30 December 2025. Downloaded on 4/29/2026 11:46:58 AM.
This article is licensed under a Creative Commons Attribution 3.0 Unported Licence.

1. Introduction

Polymeric carbon nitrides are a historic class of compounds, whose end member—accessible by thermal polymerization—was named "melon" by Liebig in 1834.[1] Carbon nitrides regained attention due to theoretical predictions in 1989 that β-C_3N_4 should be harder than diamond.[2] In 2009, interest in carbon nitrides resurged when graphitic carbon nitride (g-C_3N_4) was found to photocatalytically split water.[3]

Since then, materials collectively termed graphitic carbon nitride (g-C_3N_4), with their combined properties of chemical inertness, semiconducting behaviour, ease of synthesis and biocompatibility, have led to a variety of applications in sensing, electrochemistry, photocatalysis and biomedicine.[4–8]

Graphitic carbon nitride (also called polymeric carbon nitride, PCN) usually refers to the 1D polymer melon, which forms quasi-2D sheets *via* hydrogen bonds.[9] Besides melon, two further important members of the graphitic carbon nitride family are known: the 2D polymers poly(triazine imide) (PTI) and poly(heptazine imide) (PHI), which consist of triazine and heptazine units, respectively.[10–14]

Especially, PHI has extended the potential for applications, as it combines the unique properties of light absorption and charge storage. It is usually synthesized ionothermally in salt melts containing potassium ions, which are believed to assist in templating the formation of pores formed by six heptazine units. By irradiating this yellow material in the presence of a sacrificial electron donor, potassium poly(heptazine imide) (K-PHI) changes its color to blue. This behavior has been assigned to charge accumulation and the concomitant formation of heptazinyl radicals, but many aspects of this phenomenon still remain elusive.[15–20] This "blue state" is stable for several days under oxygen exclusion and opens up potential applications such as "dark photocatalysis",[14] solar batteries[21,22] and light-driven, autonomous PHI microswimmers.[23]

Even though g-C_3N_4 has been in the spotlight for several years now, the possibilities for applications are still expanding and becoming more diverse. PCN was recently used for bone repairing,[24] lemon-yellow dye detoxification,[25] solar-induced photocatalytic removal of antibiotics,[26] and heat transfer, using mushrooms as a green starting material.[27]

Thus, the structural design and rational modification of graphitic carbon nitrides have become increasingly important to address the desired application and to optimize performance or activity. In this regard, numerous methods have been reported, including nanostructure and heterostructure design, templating, exfoliation, doping, and co-polymerization.[28,29]

[a] *Max Planck Institute for Solid State Research, Heisenbergstr. 1, 70569 Stuttgart, Germany. E-mail: b.lotsch@fkf.mpg.de*
[b] *Department of Chemistry, University of Munich (LMU), Butenandtstr. 5-13, 81377 Munich, Germany*

© 2026 The Author(s). Published by the Royal Society of Chemistry

Open Access Article. Published on 30 December 2025. Downloaded on 4/29/2026 11:46:58 AM. This article is licensed under a Creative Commons Attribution 3.0 Unported Licence.

While all of these methods have an influence on the outcome for the desired application and a combination of these methods is probably necessary to optimize the activity, especially the surface of a material has a huge influence on its catalytic potential. Hence, the rational design of the surface of carbon nitrides is necessary to bring some applications from the lab scale to the industrial scale.[30]

Today, mainly three strategies are used to adjust the surface properties of carbon nitrides: elemental doping, co-polymerization, and post-synthetic functionalization (however, note the semantic overlap between these three strategies, which are often not clearly defined in the literature).[28,31] Elemental doping involves either the replacement of carbon or nitrogen in g-C_3N_4, or the addition of elements (or groups of elements) covalently to the edges of the structure. Oxygen,[32] carbon,[33] nitrogen,[34] phosphorus,[35] sulfur,[36] boron[37] and iodine are often used for exchanging carbon or nitrogen.[38] Examples of elements that were bonded covalently on the edge sites of the framework include fluorine,[39] boron,[40] and oxygen.[41] Even though many examples for elemental doping are known and such incorporations have positive effects for some applications, the diversity regarding surface modifications is somewhat limited by the restriction to certain chemically compatible elements.

More variety can be achieved by co-polymerization, which involves the thermal treatment of a standard carbon nitride precursor with additional (functionalized) co-monomers under typical carbon nitride synthesis conditions.[28] One challenge of this method is that it is typically conducted at high temperatures, which impedes the integration of many functional groups into the carbon nitride backbone. Thus, the first co-polymerization process that was reported exchanged one nitrogen atom of the heptazine unit with a carbon atom only.[42] Later, the exchange of two nitrogens with two carbons, namely the introduction of pyridine, was performed as well.[43] In addition, researchers were also able to extend the aromatic system of heptazine by adding different types of aryl groups.[44] Following this work, many other aromatic systems—mainly nitrogen-rich systems—were incorporated as well. Examples of functional groups used are melamine derivatives,[45] nucleobases[46] and 2,6-diaminopurine.[47] Besides the limitation of functional group variety due to the high pyrolysis temperature which leads to the decomposition of many organic compounds, another disadvantage of co-polymerization is uncontrollable side reactions, resulting in a defective carbon nitride structure.[31] Consequently, this method is less suitable for PHI and PTI, which have more ordered 2D structures.

Post-synthetic functionalization can overcome these problems. If a reliable post-synthetic procedure were available, this method could open up the possibility to design the surface of carbon nitrides by adding the desired function, and with that, pave the way for more efficient catalytic applications. However, the challenge for post-synthetic functionalization is the chemical inertness of carbon nitrides, generally leading to very low yields. Nevertheless, this hurdle can be overcome by using highly reactive organic molecules or harsh synthetic conditions. Examples are the addition of ferrocene,[48,49] quaterpyridine (qpy),[50,51] vitamin B_1,[52] aromatic heterocycles[53] and triphenylamine.[54] For PHI, only one example of functionalization has been reported, which is the conversion of surface groups to melamine under heat treatment.[55] For PTI, to the best of our knowledge, no example of a covalently added surface functional group is known, and only non-covalent modifications such as the treatment of PTI with isopropanol have been reported.[56]

Herein, we present a novel synthetic strategy for covalently bonding an organic functional group (FG) to the surface of PHI and two other graphitic and polymeric carbon nitrides, melon and PTI. As the functionalization can be pore intercalated, electrostatically bonded or covalently bonded, we explore strategies to differentiate between these scenarios. By using fluorinated FGs and analyzing the supernatant after purification steps, the removal of intercalated and non-covalently attached FGs was ensured. ^{19}F solid-state NMR (ssNMR) was used to quantify the covalently bonded surface groups. Moreover, 2D NMR spectroscopy on ^{15}N-enriched K-PHI and ^{13}C-enriched FGs demonstrates the successful introduction of a covalent linkage, thereby providing the first conclusive evidence that covalent surface functionalization is indeed feasible.

2. Results and discussion

2.1. Challenges in carbon nitride surface functionalization

Unambiguous evidence of the successful covalent functionalization of polymeric carbon nitrides is often elusive. The reason is that K-PHI—like other graphitic carbon nitrides—is a highly inert material with low accessibility. This is primarily because K-PHI is built up by layers, as shown in Fig. 1a–d. Given the low porosity of PHI, the tight stacking of the 2D layers, and the tendency of PHI crystallites to intergrow and form aggregates, the surface-to-volume ratio of PHI is low, and hence the bulk is not particularly accessible to functionalization. Therefore, a low ratio of functional groups to heptazines can be expected.

For example, the displayed idealized hexagonal sheet in Fig. 1b consists of about 1092 heptazine units with only 160 terminal groups, giving an already low surface group-to-heptazine ratio of 14.7 mol%. However, the sheets, which differ in size and homogeneity, tend to aggregate and form large secondary particles in the range of 700 to 1100 nm.[57] These particles are insoluble and inaccessible to most dissolved molecules, rendering only the exposed edges of the aggregates accessible for functionalization. On these edges, surface groups such as cyanamide or hydroxyl are present, but amine is the most dominant group according to NMR and vibrational spectroscopy.[57] Thus, the most rational target groups for functionalization are amines on the surface, while functional groups of the bulk structure, such as the bridging imide group in the pores of K-PHI, are less accessible, less reactive, and reactions with them might even damage the structure. The low solubility combined with the large tendency towards agglomeration and the variety of surface groups further lower the

© 2026 The Author(s). Published by the Royal Society of Chemistry

Open Access Article. Published on 30 December 2025. Downloaded on 4/29/2026 11:46:58 AM.
This article is licensed under a Creative Commons Attribution 3.0 Unported Licence.

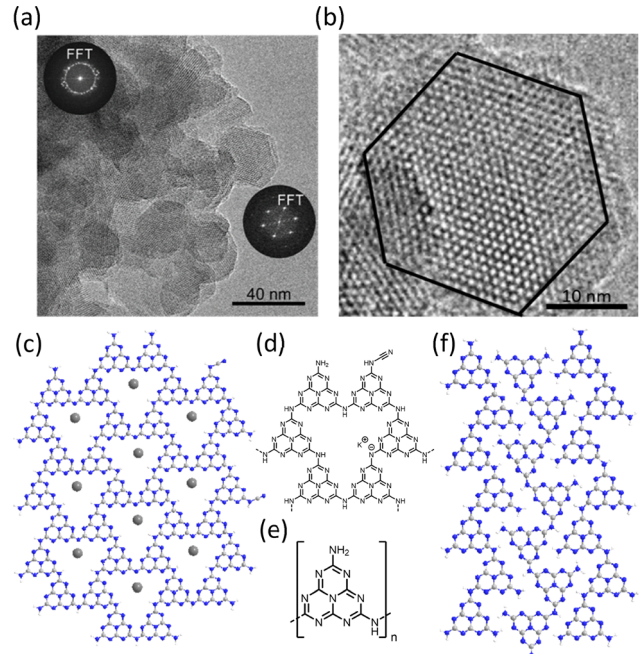

Fig. 1 TEM images (a) with an exemplary K-PHI sheet (b) and the structures of K-PHI (c and d) and melon (e and f).

expected degree of functionalization compared to the calculated ratio between surface groups and heptazines of 14.7 mol% for the idealized, single-sheet scenario. This problem is exemplified by the relation between the surface group-to-heptazine ratio of idealized spherical PHI particles with different sizes (Fig. S1). In the following, only the maximum yield for a single sheet is taken as reference, as it is more easily accessible than that for a three-dimensional, spherical particle.

In contrast to K-PHI, melon consists of 1D chains forming 2D sheets by hydrogen bonds[9] (see Fig. 1e and f). In melon, every heptazine unit carries a NH_2 group, hence the degree of functionalization should be higher compared to K-PHI. Nonetheless, this is not the case, as will be discussed in the following sections and is confirmed by reported functionalization attempts with quantified yields (Table S2). For melon, functionalization yields, given as the ratio of FG per heptazine unit, are between 0.03 and 5 mol%. Therefore, they tend to be significantly lower than the theoretical maximum functionalization yield of 14.7 mol% for K-PHI, likely due to strong in-plane hydrogen bonds, which prevent the amine groups from reacting. This suggests a quasi-2D structure, comparable to K-PHI, with reactive NH_2 groups only on the sheet edges.

Thus, for functionalizing polymeric carbon nitrides in general, low yields are expected. Three factors complicate the quantitative analysis of surface-functionalized carbon nitrides: (i) the sensitivity, as some analytical methods cannot detect low FG concentrations, (ii) assuring the complete removal of starting material to exclude the influence of unreacted FGs, and (iii) differentiating between adsorbed, electrostatically or covalently bound FGs. In this work, we chose a fluorine-containing FG owing to the high natural abundance and, hence, NMR sensitivity of ^{19}F to overcome these challenges and introduce a straightforward and fast way to screen and optimize the functionalization degree of K-PHI. In Section S5 in the SI, an evaluation of the standard analytical methods used for carbon nitrides and their functionalization is provided, along with a guideline to deal with the analytical challenges based on the findings from this work.

2.2. Functionalization method, synthetic procedure and optimization

The primary functionalization route employed in this work involves the synthesis of amides *via* a literature procedure, utilizing acyl chlorides in the presence of a base in THF.[58] To overcome the problems described above, the fluorine-containing functional group 4-(trifluoromethyl)benzoyl chloride was chosen to conduct the strategy illustrated in Fig. 2. After the reaction, the functionalized carbon nitride was thoroughly purified by suspending and centrifuging with THF and water afterwards. From each supernatant, a ^{19}F NMR spectrum was recorded for detecting unreacted FGs. Thus, by repeating the washing cycle until no fluorine NMR signal was detectable anymore, it was ensured that no starting material or physically adsorbed fluorine compound remained. For the amide-forming reaction, it usually took four washing steps with THF. The importance of this step became clear for another functionalization route, where the cyanamide group of K-PHI was functionalized with fluorine-containing phenyl rings. For the subsequent purification, 11 washing cycles were necessary to remove all non-covalently bonded fluorine compounds. A more detailed description of this synthesis and other, less successful functionalization attempts is given in the SI, with an overview in Scheme S2.

After successful purification, the solid product was investigated by ^{19}F ssNMR. The yield was quantified by adding CaF_2, as an internal standard to the functionalized carbon nitride. By this method, we were able to optimize the degree of functionalization and increase the FG-to-heptazine ratio. The results are shown in Fig. 3. The optimization of each parameter (Fig. 3a–e) was performed on the same day with the same PHI batch. The reason for using the same PHI batch is that small variations in surface groups occur between different PHI samples (see Fig. 3f and Table S1 for the standard batch deviation), which directly influence the expected yield. Furthermore, even though the amide can also be formed under aqueous conditions, water can influence the yield, as hydrolysis of the acyl chloride competes with the amide formation.[58,59] Therefore, by using starting material, solvent and dried PHI on the same day, water content variations that might affect the yield are minimized.

Firstly, the influence of different bases and temperatures was investigated (Fig. 3a). Three of the most commonly used bases (K_3PO_4, NaOH, and Et_3N) for amide formation are compared at 25 °C and 70 °C. The best base for a reaction between an acyl chloride and the amine groups of K-PHI turned out to be triethylamine. Furthermore, by increasing the temperature from 25 °C to 70 °C, the yield was increased for every base, as expected. Thus, the best result was achieved with triethylamine at 70 °C, resulting in an FG per heptazine ratio

© 2026 The Author(s). Published by the Royal Society of Chemistry

Open Access Article. Published on 30 December 2025. Downloaded on 4/29/2026 11:46:58 AM.
This article is licensed under a Creative Commons Attribution 3.0 Unported Licence.

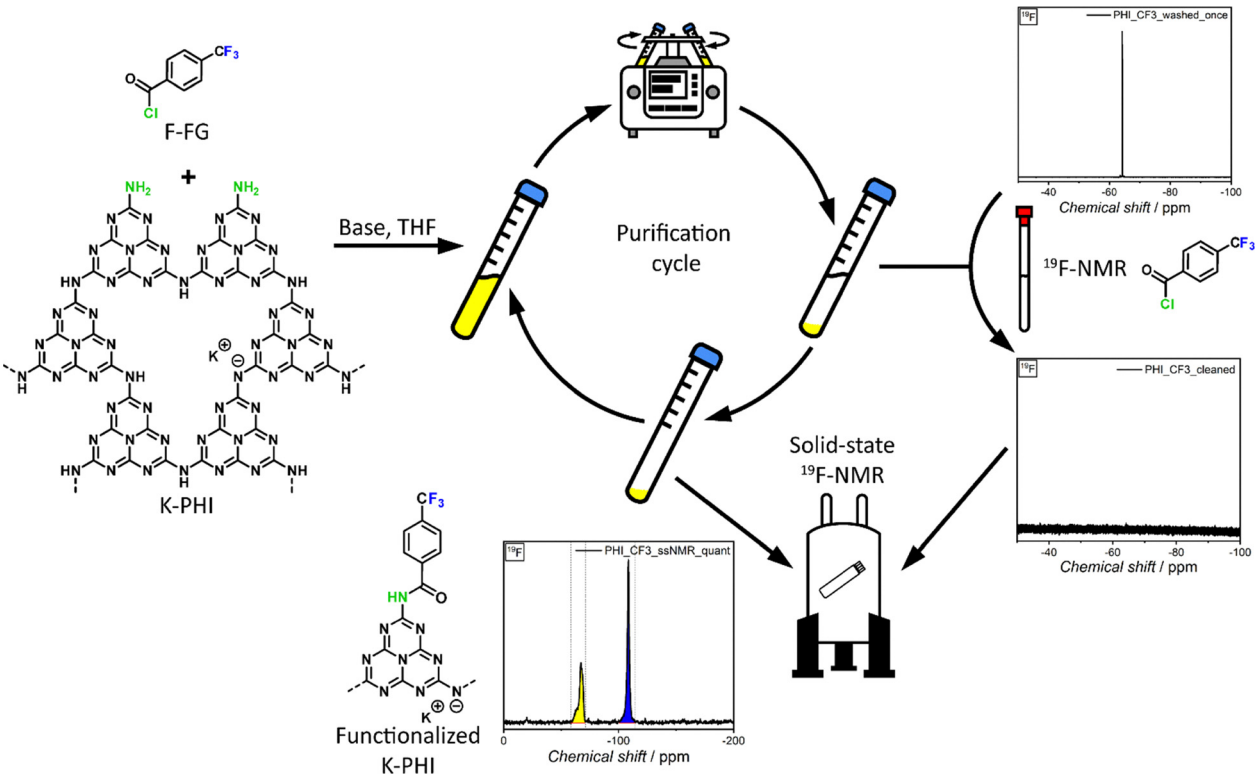

Fig. 2 Functionalization strategy for K-PHI using a fluorine-containing functional group to monitor the purification process by ^{19}F ssNMR after washing.

of 0.82 mol%. This condition was applied to the subsequent parameter optimization. The yield of 0.82 mol% FG per heptazine is already in a good range, but far away from the maximal expected yield of 14.7 mol%, symbolized by the dotted line in all figures. However, as mentioned above, this high yield would only be achievable if all surface groups were accessible and all surface groups were amine groups. Thus, the next step was to increase the amine group content of K-PHI and compare it with the carbon nitrides, containing more amine groups, *i.e.* melon and PTI (see Fig. 3b).

First, H-PHI was used instead of K-PHI, as previous studies have indicated that the treatment of K-PHI with acids leads to an increased amine content—most likely in the form of urea—(see Scheme S1), resulting from the conversion of cyanamide groups, which are present on the surface and as defects.[14,60] In line with this hypothesis, a higher surface functionalization was achieved. The same trend is visible when cyanamide groups are further converted to melamines, having two accessible amine groups for functionalization. The resulting Mel-PHI[55] achieved an FG per heptazine ratio of 1.70 mol%. Melon is built up by 1D heptazine chains with each heptazine having one amine group that forms quasi-2D sheets by hydrogen bonds. Theoretically, an FG per heptazine ratio of 100 mol% would be achievable if the chains were separated and every amine reacted with one functional group. However, for this reaction, only a yield of 0.71 mol% was reached. This is in agreement with literature values for melon functionalizations, and the reason for the low yield is described above. For PTI, which is built up by 2D triazine sheets, a yield of 0.98 mol% FG-to-triazine units was obtained (Fig. 3b). As the triazine unit is smaller than heptazine, PTI shows a denser functionalization than PHI. Its slightly higher yield than that of PHI can be explained by the presence of more amine groups as surface groups, which seem to be better accessible.

In the next step, K-PHI samples with different agglomerate sizes are compared (see Fig. 3c). For preparing different K-PHI particle sizes, a literature procedure by Kröger *et al.*[57] was used, which reports an increased surface group-to-bulk ratio for smaller K-PHI particles. Thus, higher functionalization yields can be expected for reduced particle sizes. By sonication and centrifugation, three different agglomerate size ranges were obtained: 400–650 nm for size 1, 200–400 nm for size 2, and about 200 nm for size 3, respectively. Pristine K-PHI has particle sizes larger than 650 nm. Thus, the expected trend is an increasing yield from pristine K-PHI over size 1 and 2 to size 3. This is exactly what we observe, with a degree of functionalization of 2.41 mol% for size 3. The same procedure was carried out for melon, also resulting in a higher functionalization degree for the smallest particle sizes (about 150 nm) compared to pristine melon (about 1200 nm).

Another parameter that was investigated is the time dependence for K-PHI functionalization. As visible in Fig. 3d, an optimum yield is reached after 2 h. If the reaction is not stopped at this point, the yield starts to decrease again, until a final state is reached. For melon, this is not the case. Here, the yield is slightly lower after 2 h compared to 17 h (Fig. 3f). The main difference between K-PHI and melon that might influence the reaction is the pore-adsorbed water in K-PHI. Even though dried starting materials were used, some more strongly

Open Access Article. Published on 30 December 2025. Downloaded on 4/29/2026 11:46:58 AM.
This article is licensed under a Creative Commons Attribution 3.0 Unported Licence.

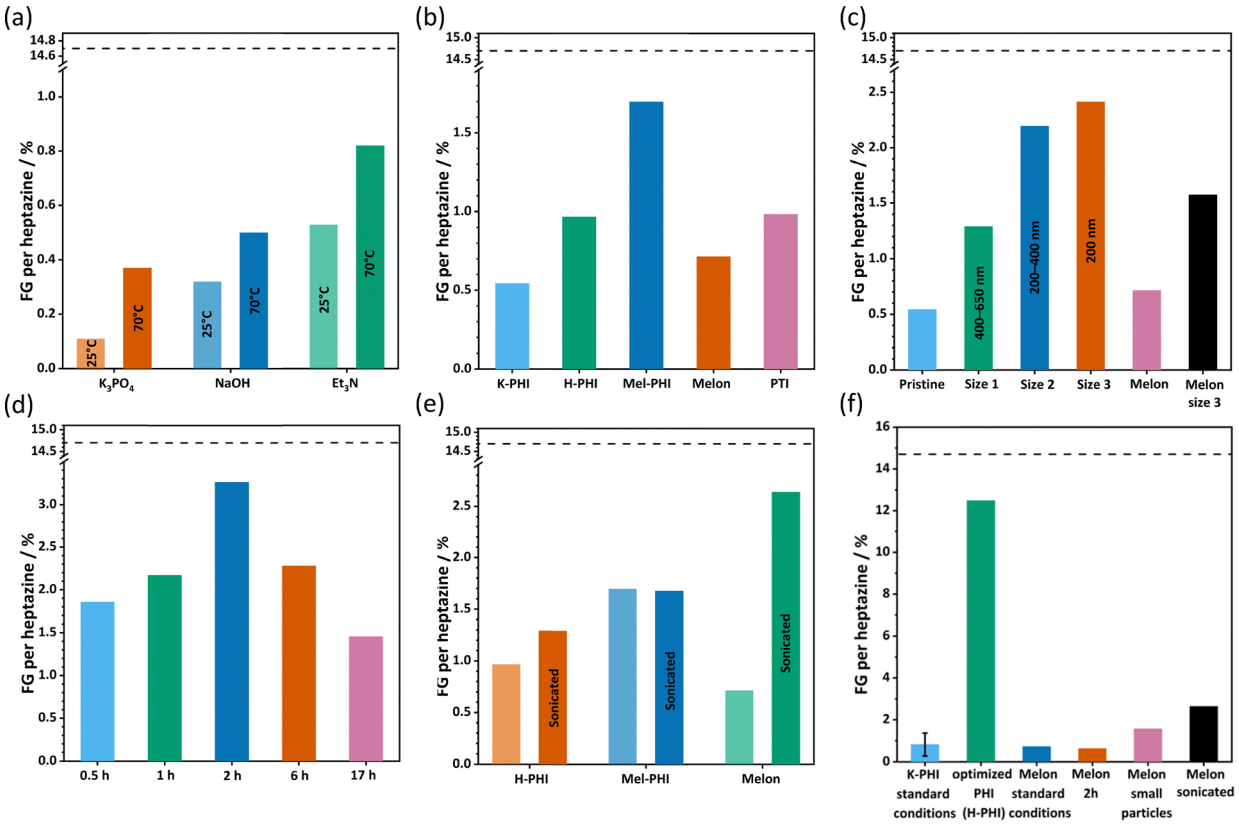

Fig. 3 Factors influencing the functionalization degree for PHI, melon, and PTI. The degree is given on a functional group-per-heptazine basis. For PTI, the degree is given in FG per triazine units for better comparison. The functionalization degrees are calculated from quantitative ^{19}F ssNMR spectroscopy. All screening experiments were done on the same day with the same batch of PHI. The reactions were conducted at 70 °C for 17 h with Et_3N, if not mentioned otherwise. The dashed line shows the maximum expected yield from an average 40-nm sheet with only amine groups on the edges and no agglomeration (and hence perfect accessibility) and a 100% reaction yield between amine groups and the acyl chloride. The screening of the following parameters is shown: (a) base and temperature. (b) K-PHI compared to H-PHI, Mel-PHI (melamine-functionalized PHI), melon and PTI. (c) Size of K-PHI and melon. (d) Time for K-PHI. (e) Influence of 30 min of sonication before the reaction. (f) Optimized conditions using H-PHI compared to the standard conditions for K-PHI with Et_3N, 70 °C and 17 h. Herein, the variance in the degree of functionalization between three distinct batches is shown as well for K-PHI. For melon, only pre-synthesis sonication without further adjustments led to the best result.

attached water is still likely present in the pores. The reaction is not very sensitive to hydrolysis.[59] However, the remaining pore water seems to influence the equilibrium after the initial reaction is completed. An explanation might be that HCl, which is formed during the functionalization reaction, along with some remaining pore water and the high temperatures, is enough to result in some hydrolysis of the newly formed amide, resulting in a more pronounced back reaction after 2 h. Despite this observation, after purification, the functionalization seems to remain stable under ambient conditions, as expected for amide bonds.

Another way to positively influence the functionalization is to sonicate the reaction mixture before heating. As shown in Fig. 3e, the yield is moderately increased for H-PHI (up to 1.29 mol%), and significantly increased for melon (up to 2.64 mol%). Apparently, by sonication, the amine groups of the carbon nitride agglomerates become better accessible for the acyl chloride. Especially for melon, with its multitude of amine groups that are inaccessible due to hydrogen bonds, sonication has a significant effect on the functionalization yield. However, for melamine-functionalized PHI, sonication does not influence the yield. This leads to the conclusion that the amine groups of Mel-PHI already are well accessible.

In Fig. 3f, the combination of optimized functionalization parameters for PHI is shown and compared to the yield of K-PHI functionalization under the condition of heating at 70 °C for 17 h with triethylamine as the base. For the optimized functionalization, size 3 (200 nm) particles of H-PHI were used, which were sonicated for 30 min before the reaction and only heated for 2 h afterwards. Following this synthetic route, a functionalization yield of 12.5 mol% was achieved, meaning that every 8th heptazine unit is functionalized. The maximum degree of functionalization for the exemplary sheet shown in Fig. 1, under the assumption that every surface group is an amine group, was 14.7 mol%. Therefore, almost the complete surface of PHI (85%) is functionalized. This also means that the yield is high enough to be detectable by standard analytical methods, which are presented in the next section.

However, for melon, the optimized parameters used for PHI did not lead to the highest degree of functionalization. Even the combination of small-sized melon and sonication did not

© 2026 The Author(s). Published by the Royal Society of Chemistry

Open Access Article. Published on 30 December 2025. Downloaded on 4/29/2026 11:46:58 AM.
This article is licensed under a Creative Commons Attribution 3.0 Unported Licence.

increase the functionalization degree. The reason is probably that due to strong hydrogen bonds in melon, the size-reduced particles agglomerate when suspended in THF. Nevertheless, sonication enhances amine accessibility in the case of melon; hence, we recommend that in addition to the standard conditions of 17-h heating time to increase the diffusivity of the reactants, an initial sonication process be used for the best results.

2.3. Characterization of the optimized sample

Under optimized conditions, a functionalization degree of 12.5 mol% was reached for protonated PHI (H-PHI). H-PHI was used, as its functionalization yield is higher compared to K-PHI. Thus, the optimized, functionalized PHI in this section does not contain potassium. However, K-PHI is occasionally mentioned for comparison as well. The functionalization yield was calculated by ^{19}F ssNMR with CaF_2 as an internal standard (see Fig. 4a). Prior to this, the functionalized product was purified thoroughly, as illustrated in Fig. 2. The ^{19}F NMR spectra of the last washing step with THF and water, respectively, are depicted in Fig. S2b. In the following, further analytical methods are used to show the successful functionalization. Due to the complete removal of soluble fluorine

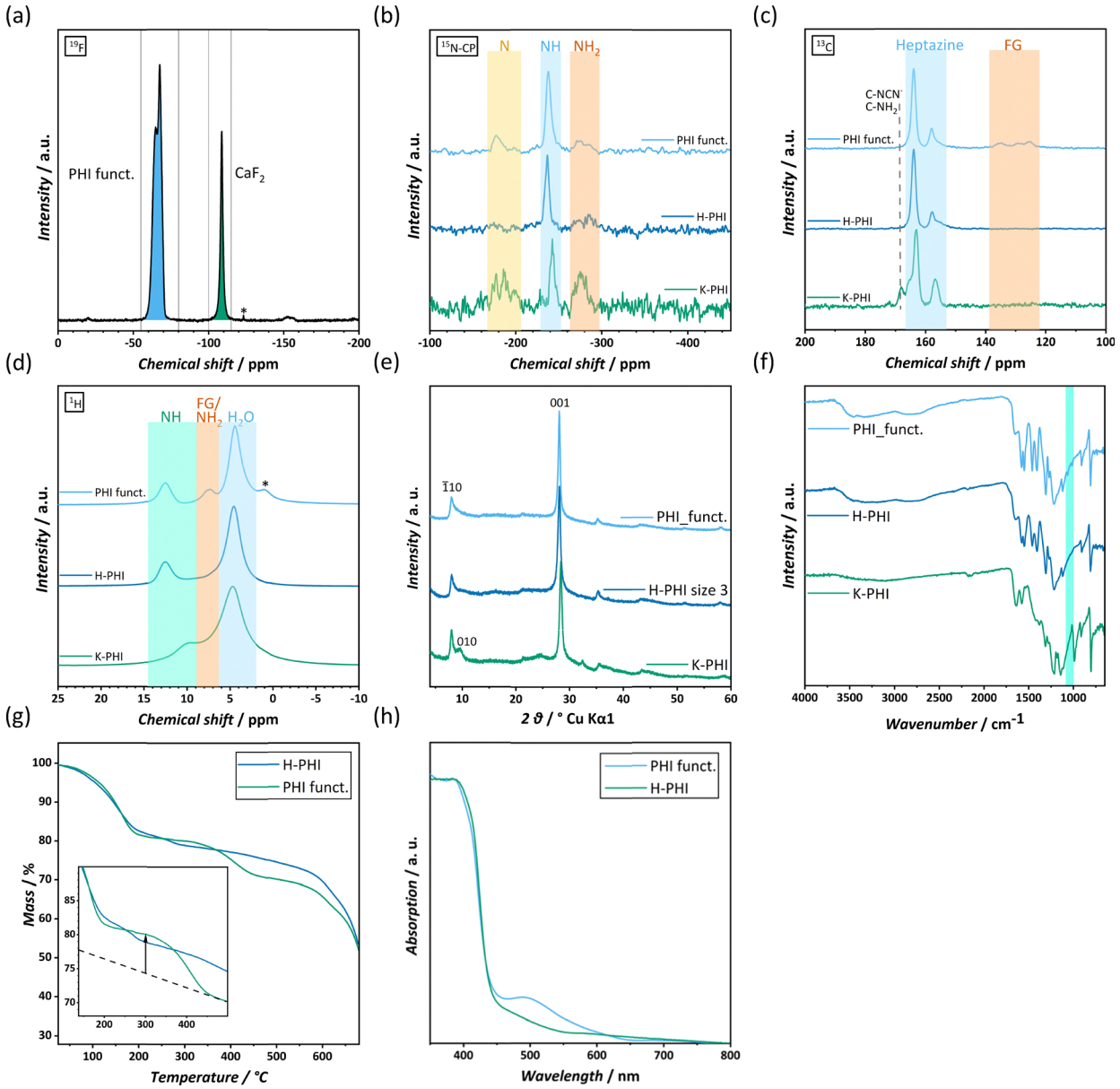

Fig. 4 Characterization of the optimized, functionalized sample (PHI funct., which is H-PHI based). (a) Determination of the degree of functionalization by ^{19}F ssNMR; (b) ^{15}N-CP ssNMR, (c) $\{^1H\}^{13}C$ ssNMR, and (d) ^{1}H ssNMR. The asterisk marks an impurity, which is assigned to residues of the pore-intercalated THF. (e) PXRD measurements and (f) IR measurements with the only region hinting towards the functionalization being highlighted. (g) TGA measurement with a close-up of the T region where the FG evaporated from CN. The dashed line shows the theoretical course of mass loss if PHI was not functionalized. From the difference, the functionalization yield was calculated. (h) UV-vis spectroscopy.

Open Access Article. Published on 30 December 2025. Downloaded on 4/29/2026 11:46:58 AM. This article is licensed under a Creative Commons Attribution 3.0 Unported Licence.

species, it is ensured that no starting material or loosely bound FGs interfere with the analysis; only covalently bound FGs are detected.

First, further ssNMR measurements of the optimized H-PHI sample compared to H-PHI and K-PHI are shown. Generally, the ^{15}N-CP NMR spectrum (Fig. 4b) of the functionalized H-PHI is in agreement with the non-functionalized H-PHI. However, the NH_2 signal for the functionalized sample is reduced in intensity compared to that for the non-functionalized materials, relative to the heptazine ring nitrogen atoms. This can be explained by the functionalization, as the free amine groups reacted with the FGs. However, it is difficult to draw clear conclusions from ^{15}N-CP NMR measurements. Better indicators for the success of functionalization are obtained by ^{13}C NMR measurements (Fig. 4c), where new signals between 122 and 138 ppm appear. Neither the herein investigated K-PHI and H-PHI samples, nor the samples reported in the literature exhibit signals in this region. The cyanamide signals are typically visible at lower chemical shifts than 122 ppm.[14,55] Thus, we assign these signals to the phenyl ring and the CF_3 group of the FG, which is in accordance with the literature NMR measurements.[61] Functionalization can also be concluded from ^{1}H NMR measurements (Fig. 4d), as the hydrogen signals of the phenyl ring from the FG group can be observed between 7.5 and 8.5 ppm. However, the loss of NH_2 groups that would also be a sign of functionalization is not detectable in the ^{1}H spectrum, as the signal overlaps with those of the FG. Nevertheless, the presence of FGs is clearly visible by additional signals in the ssNMR, which are usually not present in H-PHI.

While a change in the powder X-ray diffraction (PXRD) pattern is not expected for surface-functionalized carbon nitrides, it is useful to confirm whether the PHI backbone is still intact and crystalline. As visible in Fig. 4e, the PXRD pattern for functionalized PHI is in agreement with the patterns of K-PHI and particle-size-reduced H-PHI P3. The variation in the 010 reflection, as compared to K-PHI, is associated with the reduction in particle size, a phenomenon that has been elucidated in prior studies.[14,57]

In the IR spectrum (Fig. 4f), the intact PHI backbone is also confirmed, as the main vibrations have not changed. Additionally, hints of the functionalization are present in the region between 1000 and 1100 cm^{-1}, which are assigned to strong CF_3 stretching bands.[62] Besides, no clear evidence is visible for FGs, even though the functionalization yield is very high. This is due to the strong carbon nitride vibrations, as discussed in Section S5 in the SI.

Proof that the morphology of PHI particles was not significantly affected by the functionalization can be seen by using scanning electron microscopy (SEM) and transmission electron microscopy (TEM). Like PXRD, the TEM images (Fig. S3) show that the crystallinity of PHI is preserved, while the pore-like structure is also intact. In SEM images (Fig. S4), the small grains of the functionalized PHI are visible, while for pristine PHI, large particle agglomerates are present. This shows the previously described importance of reducing the particle size to increase the accessible surface area and increase the yield.

The effects of functionalization were further investigated by energy dispersive X-ray (EDX) measurements. In Fig. S5, the homogeneous distribution of fluorine over the material is shown. The fluorine content in the depicted area was measured to be 0.6 mol% (see Table S3). Compared to the nitrogen content, an approximate functionalization yield of 3.5 mol% was calculated. Note that the detection of elements with atomic numbers below 11 is difficult in EDX and might result in inaccurate quantification, hence explaining the lower observed degree of functionalization.[63]

A more precise functionalization degree was calculated from elemental combustion analysis (EA); see Table S4. As seen from the table, a higher carbon content was detected compared to the nitrogen content. By using the carbon/nitrogen ratio of untreated PHI and assuming that the remaining carbon amount belongs to the functionalization, a functionalization degree of approximately 13.7 ($\pm$1.1) mol% is calculated.

For thermogravimetric analysis (TGA), a mass loss caused by the FG (see Fig. 4g) is observable. The initial mass loss at temperatures below 200 °C can be assigned to pore water that is removed from H-PHI. The mass difference for untreated and functionalized H-PHI is similar. At higher temperatures, the TGA curves diverge. Between 300 and 475 °C, the functionalized sample loses 5.8% more mass than H-PHI. The functionalization degree from that loss was calculated to be 8.6 mol%. If the total loss for functionalized PHI between 300 and 475 °C is used for the calculation, a functionalization degree of 14.8 mol% results, consistent with the other measurements.

Next, X-ray photoelectron spectroscopy (XPS) measurements of functionalized PHI and the starting material are compared. In the C 1s spectrum, clear changes are visible (Fig. 5a). While the typical heptazine ring signal is still present in the functionalized PHI, the CF_3, C–C/C–H and C═O signals increase due to the functional group content. The potassium signals are absent due to protonation of K-PHI before the synthesis. In the N 1s spectra, mainly the new signal at 401.29 eV shows the successful functionalization, as it belongs to an amide bond (NH–(C═O)) (Fig. 5b). Additionally, a large increase in fluorine on the surface of PHI is visible in the F 1s spectrum (Fig. 5c). The fluorine impurities from K-PHI can be explained by residues of Teflon-containing labware or noises in general. XPS was also used for quantitative surface analysis. The relevant signals C 1s (C–C/C–H, C═O), N 1s (NH–(C═O)) and F 1s increase in the correct ratio for the functional group (see Table S5, marked blue). The only inconsistent signal is the C 1s (CF_3), which stays almost constant upon functionalization. A reason might be an overlap with another signal not belonging to CF_3. From XPS quantification for all elements (Table S5), a functionalization degree of 29.41 mol% was calculated. As the information depth for XPS is usually only about 10 nm, the value does not show the total (bulk) functionalization degree, but only the surface composition. Nevertheless, XPS analysis ascertains a substantial fluorine content at the surface and, hence, successful functionalization.

To assess the effect of surface modifications on the dispersibility in water, zeta potential measurements were performed.

© 2026 The Author(s). Published by the Royal Society of Chemistry

Open Access Article. Published on 30 December 2025. Downloaded on 4/29/2026 11:46:58 AM.
This article is licensed under a Creative Commons Attribution 3.0 Unported Licence.

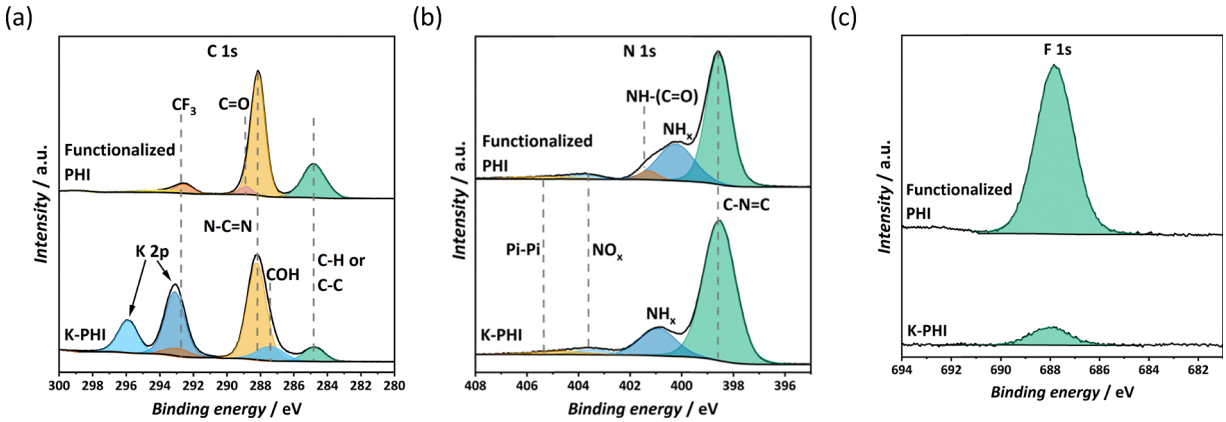

Fig. 5 XPS measurements of the functionalized PHI compared to K-PHI from different elements. (a) C 1s spectra, (b) N 1s spectra and (c) F 1s spectra.

The measured values at pH = 7 for unreacted carbon nitride are in accordance with the literature, with −45 (±2) mV for K-PHI[55] and −27 (±2) mV for particle-size-reduced H-PHI.[57] The unfunctionalized H-PHI sample was treated under the same reaction conditions as the functionalized sample, but without the FG as starting material. The functionalized sample has a zeta potential of −44 (±2) mV at pH = 7 and has thus a better suspension stability in water than H-PHI. This is attributed to the polar character of the amide group of the FG and the larger fluorine content on the surface, which is known to have a positive effect on the dispersibility.[64]

The influence on the surface properties of H-PHI caused by the functionalization can further be visualized by contact angle measurements (Fig. 6). The surface of the optimized functionalized PHI shows an increased hydrophobic behavior (52° ± 3°) compared to K-PHI (29° ± 2°) and H-PHI P3 (42° ± 1°). This was expected, as a higher fluorine content on the surface strongly increases the hydrophobicity and, hence, contact angle.[65] The functionalization effect on the surface wettability is similar to that for melamine-functionalized PHI (57° ± 9°).[55]

UV-vis spectroscopy also supports the successful functionalization, as visible by an additional absorption band at 500 nm (Fig. 4h). By ^{19}F NMR, it was ensured that the starting material was removed completely, which excludes the possibility of unreacted starting material being responsible for this absorption. The particle size reduction is also not the reason for the new absorption band in the visible region.[57] The phenomenon of additional absorption bands is discussed in more detail in Section S5 in the SI. To further investigate the influence of the functionalization, the band gap was calculated (Fig. S2a). H-PHI synthesized here has a band gap of 2.92 eV, which is in agreement with the literature. Values of size-reduced H-PHIs are similar.[57] As visible, the functionalization has no significant influence on the band gap, with a maximum change to 2.94 eV.

Altogether, the combination of analytical methods shown above confirms the presence of the FGs. Combined with the fact that loosely bound residues of FGs were removed before the measurements, the successful surface functionalization of PHI can be ascertained. However, clear proof of the newly formed covalent bond is only possible using isotopically enriched 2D NMR spectroscopy, which is discussed in the next section.

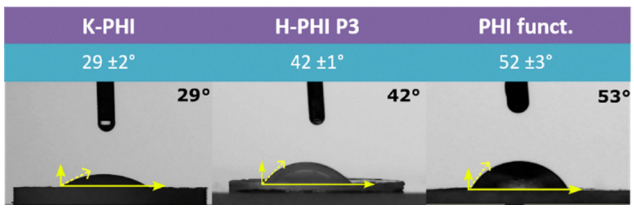

Fig. 6 Contact angle measurements of the functionalized PHI compared to H-PHI size 3 (200 nm) particles and K-PHI.

2.4. Isotopically enriched 2D ^{13}C and ^{15}N NMR

To analyze the covalent attachment of the FG to the PHI backbone, 2D ssNMR measurements were carried out.

Accounting for the low natural abundance and hence the low sensitivity of both ^{13}C and ^{15}N, ^{13}C- and ^{15}N-enriched compounds were used. For the FG, only the relevant carbon that forms the bond to the amine group of PHI was enriched. In contrast, K-PHI was completely ^{15}N-enriched to ensure that essentially all amine groups, which are relevant for bond formation with the FG, are isotopically enriched. As a significant amount of ^{15}N K-PHI was necessary for the synthesis and analysis, a new synthesis strategy was developed, where only the cheap precursor material urea was used as nitrogen source. A problem when using urea for carbon nitride synthesis is the evaporation of urea when heat is applied. This results in a huge loss of material when the starting material is heated in an open system, but on the other hand prevents large-scale synthesis in ampoules due to the high autogenous pressure that develops during the polycondensation reaction. Therefore, a safety valve was used, keeping a small pressure in the system to allow the highly reactive formed gas molecules to polymerize to more condensed carbon nitrides, while on the other hand preventing high-pressure risks resulting from large-scale (gram-scale) synthesis. Afterwards, the mixture of melon and less condensed carbon nitrides was heated with KI to obtain ^{15}N K-PHI. Subsequent protonation and size reduction of ^{15}N K-PHI were

Open Access Article. Published on 30 December 2025. Downloaded on 4/29/2026 11:46:58 AM.
This article is licensed under a Creative Commons Attribution 3.0 Unported Licence.

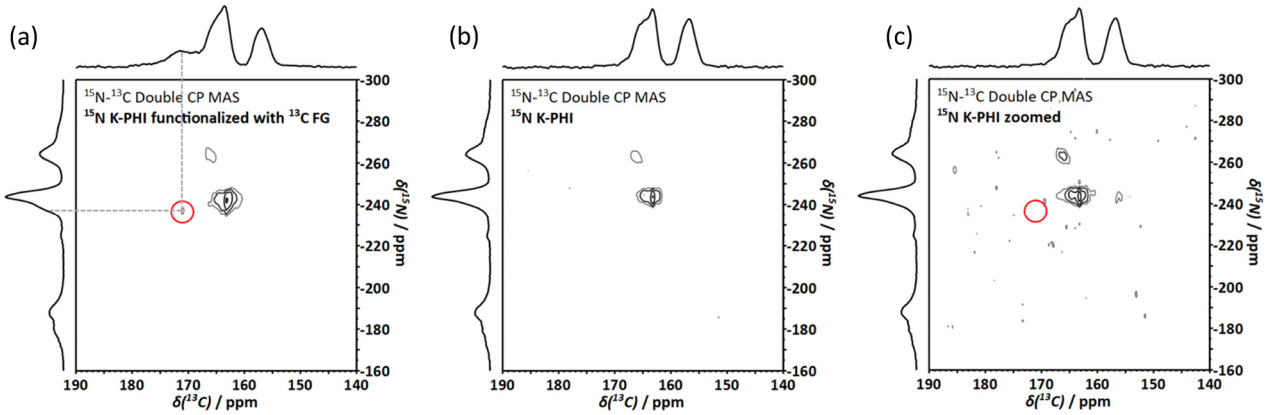

Fig. 7 ^{15}N-^{13}C double CP MAS NMR of functionalized ^{15}N-enriched K-PHI (a) compared to ^{15}N-enriched K-PHI without functionalization (b and c). The carbon atom that is bonded to the amine group is ^{13}C-enriched. (c) Scaled (zoomed) version of (b) showing higher background, and the red circle shows the missing signal that is visible in (a).

avoided in order to prevent further material loss. Thus, normal-sized, unprotonated K-PHI was used, with otherwise optimized conditions, to functionalize the isotopically enriched material.

To obtain information about the connectivities, 2D ^{15}N-^{13}C double CP MAS NMR of the ^{15}N-^{13}C-enriched functionalized K-PHI was measured and compared to the non-functionalized ^{15}N K-PHI (Fig. 7). While the 1D spectra are almost identical, an additional peak at about 171 ppm is visible in the ^{13}C spectrum of the functionalized sample. This signal can be assigned to the ^{13}C-enriched carbon of the FG. In the 2D spectrum, this peak correlates with a small side band of the amine signal of K-PHI (red circle in Fig. 7a). On the other hand, a comparable signal is not present in the 2D NMR spectrum of the unreacted PHI (Fig. 7b), even if a higher background level is shown (Fig. 7c, indicated by the red circle). We therefore conclude that the covalent surface functionalization of PHI was successful and that surface functionalizations are possible in general, despite the generally unreactive and inert character of carbon nitrides.

3. Conclusion

In this work, the first covalent functionalization of PHI with an organic molecule was demonstrated and studied, using a highly reactive acyl chloride as the functionalization agent. To overcome the combined limitations of low yield and low sensitivity of most analytical methods when determining the degree of functionalization, a fluorine-labelled reagent was used. This strategy enabled us to monitor the reaction progress of removing unreacted FGs by ^{19}F NMR analysis of the supernatant. The yield of the remaining, covalently bound fluorine-containing FG was calculated by quantitative ^{19}F ssNMR without the inconvenience of interfering atoms. Screening experiments revealed the importance of reducing the secondary particle size to increase the accessible surface area. The highest yields were reached with protonated PHI after 2 h at 70 °C with Et_3N as the base and sonication before starting the reaction. Despite the unreactive character of carbon nitrides, it was proven for the first time by utilizing 2D ssNMR on ^{15}N-enriched K-PHI, functionalized with ^{13}C-enriched benzoyl chloride, that covalent functionalization of the inert carbon nitride backbone is possible. While in this work, the functionalization of the most intensely studied graphitic carbon nitrides, PHI, melon and PTI was shown to be feasible, many hurdles are yet to be overcome to arrive at a quantitative and reproducible functionalization strategy for carbon nitrides, owing to their highly inert backbones. This work, however, sets the stage for a more comprehensive understanding of the limitations and pitfalls of carbon nitride functionalization and provides a guideline for the quantitative introduction of functional groups and their analysis. For example, care should be taken to ensure the complete removal of the starting material; to maintain structural and morphological identity and integrity; to remove or exclude non-covalently bound functional groups, and to enable quantitative analysis of the degree of functionalization. Given that our method of using acyl chlorides, combined with optimized PHI synthesis, provides a high degree of surface functionalization, we anticipate that this method will be broadly applicable to other acyl chlorides as well. In summary, the presented functionalization protocol enables the quantitative introduction and conversion of a wide range of functional groups, which has the potential to diversify the chemistry of carbon nitrides and to open up new applications where tailored selectivity and reactivity are key.

Author contributions

The experiments were conducted by F. B. and N. L. K., under the supervision of B. V. L. Data analysis was conducted by F. B., with analytical help being provided by I. M., S. D., S. B. and K. K. The manuscript was written by F. B., S. B. and B. V. L. with inputs from all other authors.

Conflicts of interest

The authors declare no conflict of interest.

© 2026 The Author(s). Published by the Royal Society of Chemistry

Open Access Article. Published on 30 December 2025. Downloaded on 4/29/2026 11:46:58 AM. This article is licensed under a Creative Commons Attribution 3.0 Unported Licence.

Data availability

The data supporting this article, along with experimental details, instrumental details, information about other functionalization strategies and a guideline for carbon nitride functionalization, have been included as part of the supplementary information (SI). Supplementary information is available. See DOI: https://doi.org/10.1039/d5ma01345c.

Acknowledgements

We gratefully acknowledge financial support by the Max Planck Society and by the Deutsche Forschungsgemeinschaft (DFG, German Research Foundation) under Germany's Excellence Strategy – EXC 2089/2 – 390776260. The authors thank V. Duppel for TEM, SEM and EDX measurements; S. Trenker for help with the ^{13}C-enriched FG synthesis; and J. Blahusch for his help with the writing process and his overall support. Open Access funding provided by the Max Planck Society.

References

1 J. Liebig, *Ann. Pharm.*, 1834, **10**, 1–47.
2 A. Y. Liu and M. L. Cohen, *Science*, 1989, **245**, 841–842.
3 X. Wang, K. Maeda, A. Thomas, K. Takanabe, G. Xin, J. M. Carlsson, K. Domen and M. Antonietti, *Nat. Mater.*, 2009, **8**, 76–80.
4 T. Banerjee, F. Podjaski, J. Kröger, B. P. Biswal and B. V. Lotsch, *Nat. Rev. Mater.*, 2020, **6**, 168–190.
5 J. Liu, H. Wang and M. Antonietti, *Chem. Soc. Rev.*, 2016, **45**, 2308–2326.
6 X. Zhang, X. Xie, H. Wang, J. Zhang, B. Pan and Y. Xie, *J. Am. Chem. Soc.*, 2013, **135**, 18–21.
7 F. Podjaski and B. V. Lotsch, *Adv. Energy Mater.*, 2020, **11**, 2003049.
8 J. R. Zhang, Y. S. Kan, L. L. Gu, C. Y. Wang and Y. Zhang, *Chem. – Asian J.*, 2021, **16**, 2003–2013.
9 B. V. Lotsch, M. Doblinger, J. Sehnert, L. Seyfarth, J. Senker, O. Oeckler and W. Schnick, *Chem. – Eur. J.*, 2007, **13**, 4969–4980.
10 E. Wirnhier, M. Doblinger, D. Gunzelmann, J. Senker, B. V. Lotsch and W. Schnick, *Chem. – Eur. J.*, 2011, **17**, 3213–3221.
11 M. J. Bojdys, J. O. Muller, M. Antonietti and A. Thomas, *Chem. – Eur. J.*, 2008, **14**, 8177–8182.
12 K. Schwinghammer, B. Tuffy, M. B. Mesch, E. Wirnhier, C. Martineau, F. Taulelle, W. Schnick, J. Senker and B. V. Lotsch, *Angew. Chem., Int. Ed.*, 2013, **52**, 2435–2439.
13 M. Doblinger, B. V. Lotsch, J. Wack, J. Thun, J. Senker and W. Schnick, *Chem. Commun.*, 2009, 1541–1543.
14 H. Schlomberg, J. Kroger, G. Savasci, M. W. Terban, S. Bette, I. Moudrakovski, V. Duppel, F. Podjaski, R. Siegel, J. Senker, R. E. Dinnebier, C. Ochsenfeld and B. V. Lotsch, *Chem. Mater.*, 2019, **31**, 7478–7486.
15 V. W.-h Lau, D. Klose, H. Kasap, F. Podjaski, M.-C. Pignié, E. Reisner, G. Jeschke and B. V. Lotsch, *Angew. Chem.*, 2017, **129**, 525–529.
16 Z. Zeng, X. Quan, H. Yu, S. Chen, Y. Zhang, H. Zhao and S. Zhang, *Appl. Catal., B*, 2018, **236**, 99–106.
17 A. Savateev, B. Kurpil, A. Mishchenko, G. Zhang and M. Antonietti, *Chem. Sci.*, 2018, **9**, 3584–3591.
18 R. Mann and D. Khushalani, *J. Mater. Chem. A*, 2023, **11**, 20601–20607.
19 G. Seo, R. Hayakawa, Y. Wakayama, R. Ohnuki, S. Yoshioka and K. Kanai, *Phys. Chem. Chem. Phys.*, 2024, **26**, 20585–20597.
20 R. Mann, R. Tyagi, K. Bhattacharyya, V. K. Voora and D. Khushalani, *Cell Rep. Phys. Sci.*, 2025, **6**, 102812.
21 F. Podjaski, J. Kroger and B. V. Lotsch, *Adv. Mater.*, 2018, **30**, 1705477.
22 A. Gouder, F. Podjaski, A. Jimenez-Solano, J. Kroger, Y. Wang and B. V. Lotsch, *Energy Environ. Sci.*, 2023, **16**, 1520–1530.
23 V. Sridhar, F. Podjaski, J. Kroger, A. Jimenez-Solano, B. W. Park, B. V. Lotsch and M. Sitti, *Proc. Natl. Acad. Sci. U. S. A.*, 2020, **117**, 24748–24756.
24 A. A. Sadek, M. Abd-Elkareem, H. N. Abdelhamid, S. Moustafa and K. Hussein, *Sci. Rep.*, 2023, **13**, 5404.
25 S. Li, P. Liu, Y. Wang, Q. Yang and Y. Ma, *Food Chem.*, 2023, **422**, 136263.
26 J. Chen, Z. Yan, Y. Chen, K. Yao and Z. Xu, *Appl. Surf. Sci.*, 2023, **634**, 157637.
27 V. Gokul, M. N. S. Swapna, G. Ambadas and S. I. Sankararaman, *Diam. Relat. Mater.*, 2023, **138**, 110215.
28 W. J. Ong, L. L. Tan, Y. H. Ng, S. T. Yong and S. P. Chai, *Chem. Rev.*, 2016, **116**, 7159–7329.
29 F. K. Kessler, Y. Zheng, D. Schwarz, C. Merschjann, W. Schnick, X. Wang and M. J. Bojdys, *Nat. Rev. Mater.*, 2017, **2**, 1–17.
30 D. K. Chauhan, S. Jain, V. R. Battula and K. Kailasam, *Carbon*, 2019, **152**, 40–58.
31 N. Wang, L. Cheng, Y. Liao and Q. Xiang, *Small*, 2023, **19**, 2300109.
32 J. Li, B. Shen, Z. Hong, B. Lin, B. Gao and Y. Chen, *Chem. Commun.*, 2012, **48**, 12017–12019.
33 G. Dong, K. Zhao and L. Zhang, *Chem. Commun.*, 2012, **48**, 6178–6180.
34 Y. Zhou, L. Zhang, W. Huang, Q. Kong, X. Fan, M. Wang and J. Shi, *Carbon*, 2016, **99**, 111–117.
35 S. Hu, L. Ma, J. You, F. Li, Z. Fan, F. Wang, D. Liu and J. Gui, *RSC Adv.*, 2014, **4**, 21657–21663.
36 G. Liu, P. Niu, C. Sun, S. C. Smith, Z. Chen, G. Q. Lu and H.-M. Cheng, *J. Am. Chem. Soc.*, 2010, **132**, 11642–11648.
37 Y. Wang, H. Li, J. Yao, X. Wang and M. Antonietti, *Chem. Sci.*, 2011, **2**, 446–450.
38 Q. Han, C. Hu, F. Zhao, Z. Zhang, N. Chen and L. Qu, *J. Mater. Chem. A*, 2015, **3**, 4612–4619.
39 Y. Wang, Y. Di, M. Antonietti, H. Li, X. Chen and X. Wang, *Chem. Mater.*, 2010, **22**, 5119–5121.
40 S. C. Yan, Z. S. Li and Z. G. Zou, *Langmuir*, 2010, **26**, 3894–3901.

© 2026 The Author(s). Published by the Royal Society of Chemistry

Open Access Article. Published on 30 December 2025. Downloaded on 4/29/2026 11:46:58 AM. This article is licensed under a Creative Commons Attribution 3.0 Unported Licence.

41 H. Wang, S. Jiang, S. Chen, D. Li, X. Zhang, W. Shao, X. Sun, J. Xie, Z. Zhao, Q. Zhang, Y. Tian and Y. Xie, *Adv. Mater.*, 2016, **28**, 6940–6945.
42 J. Zhang, X. Chen, K. Takanabe, K. Maeda, K. Domen, J. D. Epping, X. Fu, M. Antonietti and X. Wang, *Angew. Chem., Int. Ed.*, 2010, **49**, 441–444.
43 Z. Chen, P. Sun, B. Fan, Q. Liu, Z. Zhang and X. Fang, *Appl. Catal., B*, 2015, **170–171**, 10–16.
44 J. Zhang, G. Zhang, X. Chen, S. Lin, L. Mohlmann, G. Dolega, G. Lipner, M. Antonietti, S. Blechert and X. Wang, *Angew. Chem., Int. Ed.*, 2012, **51**, 3183–3187.
45 M. Zhang, Y. Duan, H. Jia, F. Wang, L. Wang, Z. Su and C. Wang, *Catal. Sci. Technol.*, 2017, **7**, 452–458.
46 C. Yang, B. Wang, L. Zhang, L. Yin and X. Wang, *Angew. Chem., Int. Ed.*, 2017, **56**, 6627–6631.
47 A. Hayat, M. U. Rahman, I. Khan, J. Khan, M. Sohail, H. Yasmeen, S. Y. Liu, K. Qi and W. Lv, *Molecules*, 2019, **24**, 1779.
48 X. Ye, Y. Zheng and X. Wang, *Chin. J. Chem.*, 2014, **32**, 498–506.
49 K. A. Lin and J. T. Lin, *Chemosphere*, 2017, **182**, 54–64.
50 B. Ma, G. Chen, C. Fave, L. Chen, R. Kuriki, K. Maeda, O. Ishitani, T. C. Lau, J. Bonin and M. Robert, *J. Am. Chem. Soc.*, 2020, **142**, 6188–6195.
51 Y. Wei, L. Chen, H. Chen, L. Cai, G. Tan, Y. Qiu, Q. Xiang, G. Chen, T. C. Lau and M. Robert, *Angew. Chem., Int. Ed.*, 2022, **61**, e202116832.
52 A. Rashidizadeh, H. Ghafuri, H. R. Esmaili Zand and N. Goodarzi, *ACS Omega*, 2019, **4**, 12544–12554.
53 J. Tian, L. Zhang, X. Fan, Y. Zhou, M. Wang, R. Cheng, M. Li, X. Kan, X. Jin, Z. Liu, Y. Gao and J. Shi, *J. Mater. Chem. A*, 2016, **4**, 13814–13821.
54 C. Zhang, J. Liu, X. Liu and S. Xu, *Catal. Sci. Technol.*, 2020, **10**, 1609–1618.
55 J. Kröger, A. Jiménez-Solano, G. Savasci, P. Rovó, I. Moudrakovski, K. Küster, H. Schlomberg, H. A. Vignolo-González, V. Duppel, L. Grunenberg, C. B. Dayan, M. Sitti, F. Podjaski, C. Ochsenfeld and B. V. Lotsch, *Adv. Energy Mater.*, 2020, **11**, 2003016.
56 C.-H. Chen and K.-S. Chang, *J. Electron. Mater.*, 2019, **49**, 1518–1526.
57 J. Kröger, A. Jiménez-Solano, G. Savasci, V. W. H. Lau, V. Duppel, I. Moudrakovski, K. Küster, T. Scholz, A. Gouder, M. L. Schreiber, F. Podjaski, C. Ochsenfeld and B. V. Lotsch, *Adv. Funct. Mater.*, 2021, **31**, 2102468.
58 L. Zhang, X.-j Wang, J. Wang, N. Grinberg, D. Krishnamurthy and C. H. Senanayake, *Tetrahedron Lett.*, 2009, **50**, 2964–2966.
59 C. A. G. N. Montalbetti and V. Falque, *Tetrahedron*, 2005, **61**, 10827–10852.
60 D. D. Nekrasov, *Russ. J. Org. Chem.*, 2004, **40**, 1387–1402.
61 O. Akiko, M. Katsuya, O. Hideaki and Y. Noriyuki, *Synth. Commun.*, 2007, **37**, 2701–2715.
62 M. A. Even, S.-H. Lee, J. Wang and Z. Chen, *J. Phys. Chem. B*, 2006, **110**, 26089–26097.
63 J. Hamuyuni, M. O. Daramola and O. O. Oluwasina, *Encyclopedia of Physical Organic Chemistry*, 1st edn, 2017, pp. 1–23.
64 Z. Tang, P. Liu, J. Guo, Z. Su and C. Yang, *Appl. Surf. Sci.*, 2008, **255**, 2125–2128.
65 S. M. Mukhopadhyay, P. Joshi, S. Datta and J. Macdaniel, *Appl. Surf. Sci.*, 2001, **201**, 219–226.

© 2026 The Author(s). Published by the Royal Society of Chemistry